





Technical Note

# Algorithm for the Weak Target Joint Detection and Ambiguity Resolution Based on Ambiguity Matrix

Yitong Mao<sup>1,2</sup>, Chong Song<sup>1,3,\*</sup>  and Bingnan Wang<sup>1,2</sup> 

<sup>1</sup> National Key Laboratory of Microwave Imaging Technology, Aerospace Information Research Institute, Chinese Academy of Sciences, Beijing 100094, China; maoyitong22@mails.ucas.ac.cn (Y.M.); wbn@mail.ie.ac.cn (B.W.)

<sup>2</sup> School of Electronic, Electrical and Communication Engineering, University of Chinese Academy of Sciences, Beijing 100049, China

<sup>3</sup> State Key Laboratory of Remote Sensing Science, Institute of Remote Sensing and Digital Earth, Chinese Academy of Sciences, Beijing 100101, China

\* Correspondence: songchong@aircas.ac.cn

**Abstract:** The looking-down mode of space airship bistatic radars faces complex sea–land clutter, and the mode of wide-range surveillance and the over-sight detection of the satellite platform generates a low SNR and range–Doppler ambiguity. The method traditionally used involves the transmission of multiple Pulse Repetition Frequencies (PRFs) and correlating them to solve the ambiguity. However, with a low SNR, the traditional disambiguation fails due to the large number of false alarms and target omissions. In order to solve this problem, a new algorithm for multi-target joint detection and range–Doppler disambiguation based on an ambiguity matrix is presented. Firstly, all possible state values corresponding to the ambiguous sequence are filled into the ambiguity matrix one by one. Secondly, the state values in the matrix cell are divided into several groups of subsequences according to the PRF. By disambiguating multiple sets of subsequences, performing subsequence fusion, and then undertaking point aggregation, the targets can be effectively detected in scenarios with a strong clutter rate, the false alarms can be suppressed, and the disambiguation of the range and Doppler is completed. The simulation shows that the proposed algorithm has the strong ability to detect targets and perform ambiguity resolution in the scenario of a multi-target and multi-false alarm.



**Citation:** Mao, Y.; Song, C.; Wang, B. Algorithm for the Weak Target Joint Detection and Ambiguity Resolution Based on Ambiguity Matrix. *Remote Sens.* **2024**, *16*, 1597. <https://doi.org/10.3390/rs16091597>

Academic Editor: Ali Khenchaf

Received: 28 February 2024

Revised: 24 April 2024

Accepted: 26 April 2024

Published: 30 April 2024



**Copyright:** © 2024 by the authors. Licensee MDPI, Basel, Switzerland. This article is an open access article distributed under the terms and conditions of the Creative Commons Attribution (CC BY) license (<https://creativecommons.org/licenses/by/4.0/>).

**Keywords:** multi-target; weak target; range ambiguity; Doppler ambiguity; ambiguity matrix

## 1. Introduction

In recent years, a major breakthrough has been made in the overall design and key technologies utilized in stratospheric airship technology, which has significantly improved the long-endurance and controllable flight capabilities of the stratospheric airship platform [1]. The looking-down mode of the space airship bistatic radar for the detection and tracking of aerial targets has received much attention in recent years. In order to perform the target detection task, the radar adopts a Pulse Doppler (PD) radar system and a space echo dual-base configuration. PD radar is a combination of Doppler measurement radar and pulse radar, which has the ability to measure the distance and velocity of the target. The distance measurement of the target is obtained by measuring the time difference between the transmitted wave and the echo in the time domain, and the velocity measurement of the target is obtained by using the Doppler effect of the echo in the frequency domain [2]. Due to the large detection range of radar and the long signal propagation path, this process cannot avoid ambiguity [3,4] and the problems associated with a low signal-to-noise ratio [5].

For range and Doppler ambiguity, a universal and effective solution is to expand the detection range by using multiple PRF staggered working methods; that is, by sequentially transmitting multiple PRFs, a target can obtain different ambiguous measurements under

each PRF. This means that the target ambiguity problem is transformed and used to solve the congruent equations and that a greater degree of tactical flexibility in target detection can be achieved by using a combination of the HPRF, MPRF, and LPRF working modes [5–7]. Classical ambiguity resolutions, such as the Chinese Remainder Theorem (CRT) [8,9], can transform the state ambiguity problem under multiple PRFs into congruence equations and obtain the number of ambiguities by analyzing the solution of the equations. The one-dimensional clustering (1DC) algorithm [3,10–13] determines the number of ambiguities by performing searches and tests according to prior information. Other methods include the Hovanessian algorithm [14] and the residual look-up table (RLUT) method [15–19]. However, the traditional method increases the total time required for search or surveillance and may generate ghost or false targets in the presence of multiple targets [20].

The traditional detection algorithms utilized in Pulse Doppler radars mainly comprise two steps, namely threshold detection and ambiguity resolution [21]. Point measurements are generally first obtained by thresholding raw echo data, and the disambiguation algorithms are used for ambiguity resolution. When the SNR is low and there are multiple targets, the detection threshold of the raw echo data needs to be set low enough that more target information can be retained. However, this can generate many false alarms, resulting in complex data association problems. In addition, fluctuations in the RCS and the nonlinear motion of the targets will lead to the target being missed, which will then lead to the failure of the ambiguity resolution algorithm. PD radars that operate in the mode with multiple PRFs experience problems associated with both range ambiguity and Doppler ambiguity; therefore, to obtain the range and velocity of the target, the range and Doppler ambiguity need to be resolved. The two types of ambiguity problems are usually carried out serially; that is, the range ambiguity is solved first, and then the Doppler ambiguity is solved on this basis [22]. The traditional method of dividing range and Doppler ambiguity into two stages and resolving them one by one is tedious in algorithm design. It is worth mentioning that the causes of range and Doppler ambiguity are very similar, so the range and Doppler ambiguity can be resolved at the same time. Compared with the traditional ambiguity resolution algorithm, the proposed algorithm extends the ambiguity resolution task to the multi-target and multi-false alarm scenario. And, the algorithm considers the three problems of false alarm suppression, range, and Doppler ambiguity resolution in the same framework. Three problems associated with the task of target tracking, which is based on the looking-down mode of the space airship bistatic radar, can be solved. Firstly, for the complex data association problem caused by a large number of false alarms, the ambiguity matrix is used to block the measurement sequences. Secondly, the data association error is analyzed using the multi-dimensional observation results to realize the effective suppression of false alarms. Thirdly, by combining multi-frame and multi-PRF information, the resolution of range and Doppler ambiguity is realized.

This paper is arranged as follows: the multiple-PRF system and measurement model are developed in Section 2. In Section 3, the proposed algorithm and its procedure are presented. Moreover, the experimental parameters and results are analyzed in Section 4, and Section 5 concludes this study.

## 2. System and Models

Assuming that a multiple-PRF (suppose that  $N$  PRFs work alternately to detect the target and realize the disambiguation) radar works in the track-while-scan (TWS) mode, with  $R_{ui}$  and  $F_{vui}$  being the maximum detection range and Doppler of the radar, respectively [23], the working mode of the radar is as follows: Firstly, a coherent train of  $p_1$  pulses are transmitted at  $PRF_1$  within a coherent processing interval (CPI). Then, the next CPI is transmitted at  $PRF_2$ , and the whole process starts from scratch until  $N$  PRFs are transmitted alternately from  $PRF_1$  to  $PRF_N$ .

### 2.1. System and Measurement Models

In order to be concise, we first introduce the notations associated with range and Doppler ambiguities.

The radar adopts the satellite–airship bistatic configuration. In this configuration, both the satellite’s transmitting platform and the airship’s receiving platform are approximately stationary. The electromagnetic wave is emitted by the satellite and reflected after reaching the target; then, the stratospheric airship is responsible for receiving it. The formation of ambiguity is different from that observed on the traditional bistatic platform. The path length from the satellite to the different targets is almost the same; therefore, it seems that the error is fixed.

The motion relationship of the target relative to the transmitting station and the receiving station is shown in Figure 1. The radial velocity of the target and satellite transmitting platform and the airship receiving platform are  $v_T$  and  $v_R$ . The slant distances between the target and satellite transmitting platform and the airship receiving platform are  $R_T$  and  $R_R$ . The wavelength of the radar signal is  $\lambda$ , the PRF is  $F_r = 1/T_r$ , and  $c$  represents the propagation speed of light. The maximum unambiguous range corresponding to  $F_r$  is  $R_{ui} = cT_r$ . According to the Nyquist sampling theorem, the maximum unambiguous Doppler frequency is  $F_{vui} = F_r/2$ . When the satellite transmitting platform is relatively high, the radial velocity of the target relative to the satellite transmitting platform is approximately 0, that is,  $v_T = 0$ ; then, the relationship between the Doppler frequency shift and the Doppler velocity of the target is  $F_d = v_R/\lambda$ , and the maximum unambiguous velocity is  $v_{max} = \lambda F_{vui}/2$ .

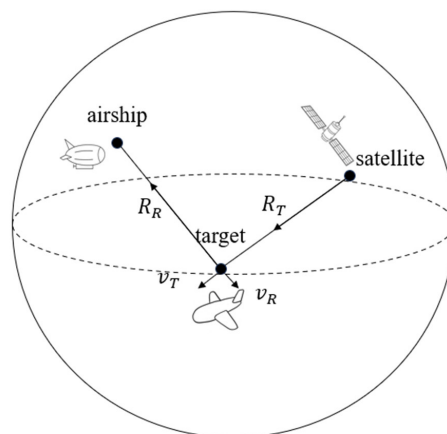


**Figure 1.** The motion relationship of the target relative to the airship and satellite.

Assume that the received measurement at each CPI is discretized based on range resolution  $\Delta_r$  and Doppler resolution  $\Delta_v$ . According to the previous description, there are a total number of  $N$  CPIs transmitted in the whole area. Therefore, the discretized measurements of  $k$ th ( $k = 1, \dots, K$ ) scan can be given as

$$\left\{ z_k(r, v) : r = \left( 1, 2, \dots, \left\lfloor \frac{R_{ui}}{\Delta_r} \right\rfloor \right), v = \left( 1, 2, \dots, \left\lfloor \frac{\lambda F_{vui}}{2\Delta_v} \right\rfloor \right) \right\} \quad (1)$$

where  $\lfloor \cdot \rfloor$  is rounded down.

The evolution of the target state can be described as a first-order Markov process represented by

$$x_{k+1}^m = f(x_k^m, n_k^m) \quad (2)$$

where  $f$  is a known function of the target state at the  $k$ th scan and  $n_k^m$  is the process noise. For example, a commonly used linear model of function  $f$  is the constant velocity (CV) model outlined below:

$$x_{k+1}^m = f(x_k^m, n_k^m) = Fx_k^m + n_k^m \quad (3)$$

where  $F$  is the state transition matrix:

$$F = \begin{bmatrix} 1 & T_s \\ 0 & 1 \end{bmatrix} \otimes I_2 \quad (4)$$

where  $I_2$  is a  $2 \times 2$  identity matrix,  $\otimes$  is the Kronecker product, and  $T_s$  is the time interval between successive measurement scans.

## 2.2. Target Model

The purpose of the algorithm is to estimate the number and state of the targets through the measurements obtained by the receiving system. In order to accurately describe the relationship between the state space of the target and the measurement space of radar observations, the standard multi-target observation model is considered [24,25]. At time  $t$ , the target  $m$  may generate a measurement with the probability of  $P_t(x_k^m, v_k^m)$  and miss detection with the probability of  $1 - P_t(x_k^m, v_k^m)$ . It is assumed that the detection probability is independent of the target state, as follows:

$$P_t(x_k^m, v_k^m) = P_t \quad (5)$$

The false alarm process can be expressed as a Poisson process, as follows:

$$\kappa(Z) = e^{-\lambda} \prod_{z \in Z} \lambda c(z) \quad (6)$$

Each scan generates an average of  $\lambda$  false alarm points; that is, the false alarm rate obeys the Poisson distribution with the parameter  $\lambda$ . The spatial distribution obeys the uniform distribution of  $c(z)$ . The intensity function is

$$\kappa_{k+1}(z) = \lambda \cdot c_{k+1}(z) \quad (7)$$

## 3. Proposed Algorithm Procedure

There are three characteristics in the looking-down mode of the space airship bistatic radar for the detection of aerial targets. Firstly, a large detection area means that the radar cannot avoid range and Doppler ambiguity problems. Secondly, the state and number of targets are constantly changing. When the number of targets increases, the complexity of data association increases, which poses a great challenge to the processing performance of the system. Therefore, data association has become a problem that must be paid attention to. Thirdly, due to the low SNR ratio, the target and the false alarm are mixed together, and the system cannot distinguish whether the observation is from the target, so it is necessary to suppress the false alarms.

The traditional method used to resolve ambiguity first correlates the measurement sequences at each PRF to obtain the number of targets and then disambiguates each target. When the number of targets is large, this method will fail due to the complexity of data association. What is more, as the weak targets are usually overwhelmed by clutter and noise at a low signal-to-clutter ratio (SCR), it is difficult to distinguish the targets and false alarms by single-frame data.

In this paper, multiple frames are processed at the same time to suppress the clutter [26]. The multi-frame joint detection and ambiguity resolution task is divided into several sub-tasks, which improves the efficiency of the algorithm [27].

The algorithm framework is shown in Figure 2. The input is the measurement sequences after CFAR detection. Take the  $K$  frame under  $N$  sets of PRF as an example. Firstly, in order to deal with the problem of ambiguity, the algorithm transforms the ambiguous measurements into network structure sequences, and then we obtain the disambiguated subsequences  $\{\tilde{X}_1^K, \tilde{X}_2^K, \dots, \tilde{X}_N^K\}$ . Secondly, the problem of false alarms and target missing will be processed by associating multi-frame measurements. We obtain the state estimation

$\{\tilde{X}_{1:N}^{\sim K}, \tilde{X}_{2:N+1}^{\sim K}, \dots, \tilde{X}_{N:2N}^{\sim K}\}$ . After the above steps, the data in the measurement space have been transformed into the state space. The target estimation result at each moment has been obtained.

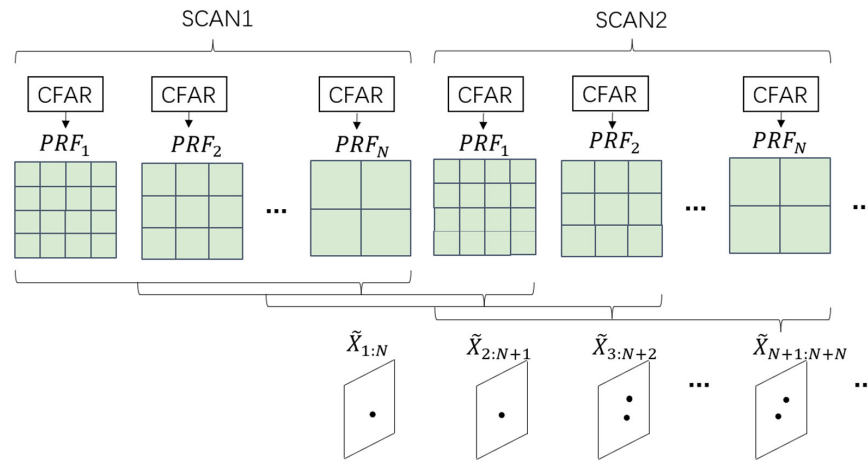


Figure 2. The workflow of the joint detection and disambiguation algorithm.

The specific implementation process of the proposed disambiguation method is represented by the pseudo-code of Algorithm 1.

**Algorithm 1:** DisambiguationDetection()

```

1  Notation: measurement  $M = [r, v]$ ; state sequence  $S$ ; maximal unambiguous range  $R_{ui}$ ;
   maximal unambiguous velocity  $v_{ui}$ ; maximal detection range  $R_{ttl}$ ; maximal detection
   velocity  $v_{ttl}$ ; position matrix range dimension length  $l_r$ ; position matrix velocity dimension
   length  $l_v$ ; prediction subsequences of moment 1 to moment  $k$   $prd_{1:k}$ ; number of PRFs  $N$ ;
   current PRF measurement sequence  $M$ ; association cut-off threshold  $e$ .
2  Input:  $prd_{1:k-1}, M$ ;
3  Output: Current frame subsequences:  $prd_{1:k}$ ;
4   $Matrix = MatrixDelete(K)$ ;
5  for  $k$  in  $M$ 
6     $S = StateReconstruct(M, R_{ui}, v_{ui}, R_{ttl}, v_{ttl})$ ;
7    for  $s$  in  $S$ 
8       $Matrix = FillinMatrix(s, l_r, l_v)$ ;
9    end for
10 end for
11 for  $i$  in  $MatrixRow$ 
12   for  $j$  in  $MatrixCol$ 
13    for  $k$  in  $N$ 
14      $prd_k = AssociationErrorCalculation(Matrix(i, j), k, e)$ ;
15    end for
16   end for
17 end for
18  $prd_{1:k} = PointCondensation(prd_{1:k-1}, prd_k, e)$ ;

```

The specific steps of the algorithm are analyzed below.

3.1. State Reconstruct

The relationship between the ambiguous measurement  $R_i$  and the actual state  $R$  of the target is  $R_i = [R]_{R_{ui}^i}$ , where the notation  $[\cdot]_a$  denotes the modulo  $a$ . The maximum range that can be detected by radar is divided into several range units according to the frequency

of each pulse repetition. Each ambiguous measurement corresponds to multiple possible actual target values  $R$ . Under  $N$  PRFs, all possible range values are shown as follows:

$$\begin{cases} R = R_1 + i \times R_{u1} \quad (i = 0, 1, \dots, u1) \\ R = R_2 + i \times R_{u2} \quad (i = 0, 1, \dots, u2) \\ \dots \\ R = R_N + i \times R_{uN} \quad (i = 0, 1, \dots, uN) \end{cases} \quad (8)$$

At each PRF, due to the ambiguity problem, the radar's maximum detection range is divided into several range–Doppler units. Each ambiguous measurement corresponds to multiple possible states  $R_{true} = [r, v]$ . If  $PRF_i$  contains  $N$  range ambiguity units and  $M$  Doppler ambiguity units, the maximum unambiguous range  $R_u$ , and the maximum unambiguous Doppler velocity  $V_u$ , then all possible states that correspond to the ambiguous state  $R = [r, v]$  and were obtained by the  $PRF_i$  are represented by the following matrix:

$$\begin{bmatrix} [r, v] & \dots & [r, v + V_u \cdot M] \\ \vdots & \ddots & \vdots \\ [r + R_u \cdot N, v] & \dots & [r + R_u \cdot N, v + V_u \cdot M] \end{bmatrix} \quad (9)$$

### 3.2. Ambiguity Matrix

In order to reduce the complexity of data association in the process of ambiguity resolution, it is necessary to divide the measurement sequences into blocks. By constructing a 2D ambiguity matrix  $T$  in which the row and column are designed according to the range and velocity scope [28], the row and column length can be obtained:

$$T_{row} = \text{ceil}\left(\frac{2BR_{max}}{c}\right) \quad (10)$$

$$T_{col} = \text{ceil}\left(\frac{2v_{max}T_{CPI}}{\lambda}\right) \quad (11)$$

where  $c$  is the propagation speed of the electromagnetic wave in free space. However, the method based on this matrix does not consider the boundary of the matrix. It is necessary to expand the boundary of the matrix region so that it is overlapped.

It can be seen from Figure 3 that, due to the error between the real states of the target and the measurements, when the targets approach the boundary of the matrix region, the measurement of the same target will be distributed in different matrix regions at different PRFs.

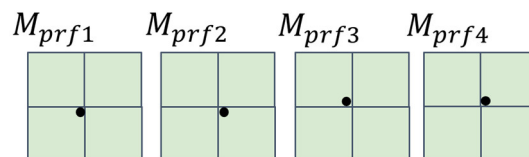


**Figure 3.** The boundary effect diagram of the matrix.

The range and Doppler velocity resolution are determined by the receive system bandwidth  $B$ , carrier wavelength  $\lambda$ , and coherent processing interval  $T_{CPI}$ , independent of pulse repetition frequency  $F_{PRF}$ . It is assumed that the range of distance error between the measurement generated by the known target and the actual value of the target is  $[-\Delta_r, \Delta_r]$ ; if the range of the velocity error is  $[-\Delta_v, \Delta_v]$ , then the width of the matrix boundary is defined as follows:

$$\text{Length}_{row} = \text{ceil}\left(\frac{2BR_{max}}{c}\right) + 2\Delta_r \quad (12)$$

$$Length_{col} = \text{ceil}\left(\frac{2v_{max}T_{CPI}}{\lambda}\right) + 2\Delta_v \tag{13}$$

### 3.3. Correlation Error and Threshold Decision

Because the radar carrier frequencies and observation angles are approximately equal in a group of PRFs, the fluctuations in the amplitude of the real target can be ignored.

If the target range error is approximately  $[-\Delta_r, \Delta_r]$  and the velocity error range is  $[-\Delta_v, \Delta_v]$ , then the normalized state is  $y_i = [r_i / (2\Delta_r), v_i / (2\Delta_v)]$ . For  $n$  states obtained at different PRFs, the association error is defined as follows:

$$RMSE = \sqrt{\frac{1}{n} \sum_{i=1}^n (\hat{y}_i - y_i)^2} \tag{14}$$

As shown in Figure 4, the algorithm distinguishes the targets and false alarms according to the determination of the association error threshold.

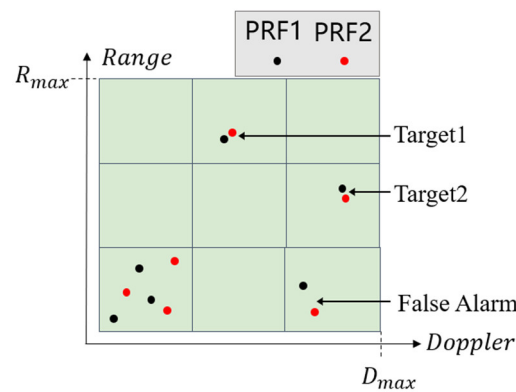


**Figure 4.** Schematic diagram of the method proposed to distinguish targets and false alarms.

Assuming that the error range of the targets is known, the threshold is set to only take the average value of the measurement sequence whose correlation error is less than the threshold; this is then used as the prediction.

The pseudo-code of Algorithm 2 represents the association threshold decision.

---

**Algorithm 2:** AssociationErrorCalculation ()

---

```

1  Notation: state sequence  $S = [r, v]$ ; PRF's index  $k$ ; number of PRFs  $n$ ; association cut-off
   threshold  $e$ ; measurement  $M(i, j)$ 
2  Input:  $M(i, j), e, n$ ;
3  Output:  $prd$ ;
4   $M = \text{deleteS}(n)$ ;
5  for  $i$  in  $S$ 
6     $r_{prd} = \frac{1}{K-1} \sum_{i=1}^{K-1} r_i$ ;
7     $v_{prd} = \frac{1}{K-1} \sum_{i=1}^{K-1} v_i$ ;
8     $r_{err} = \frac{1}{K-1} \sum_{i=1}^{K-1} (r_i - r_{prd})$ ;
9     $v_{err} = \frac{1}{K-1} \sum_{i=1}^{K-1} (v_i - v_{prd})$ ;
10   if  $\frac{r_{err}}{2\Delta_r} + \frac{v_{err}}{2\Delta_v} < e$ 
11      $prd = [r_{prd}, v_{prd}]$ ;
12   end if
13 end for

```

---

### 3.4. Point Condensation

The target state and the target prediction state do not exhibit one-to-one correspondence. In fact, because the strategy used to disambiguate and detect subsequences divides the sequence into multiple groups for calculation, a target may appear in different predicted sequences. The corresponding relationship is as follows:

$$X_{true} = \{X_{prd1}, X_{prd2}, \dots, X_{prdK}\} \quad (15)$$

In addition, due to the boundary effect of the ambiguity matrix, a measurement point may be divided into multiple matrix regions at the same time for the calculation of the correlation error; this may lead to a target possessing multiple prediction states.

Based on the above inference, the target state that is predicted by the algorithm often contains many repeated state values. The Figure 5 shows that the repeated values of the predicted target state sequence need to be filtered and merged.

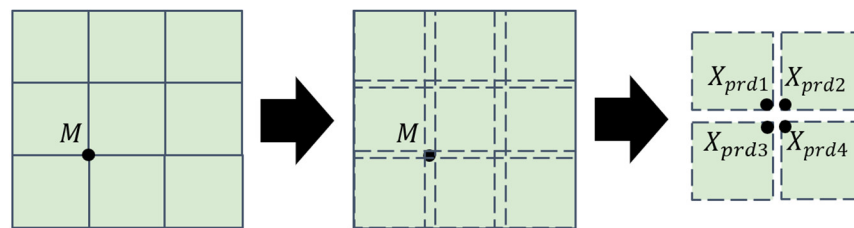


**Figure 5.** The point at the edge of the matrix region may produce four predictions.

The pseudo-code of Algorithm 3 represents the point condensation of the prediction.

---

#### Algorithm 3: PointCondensation()

---

```

1  Notation: state prediction  $prd_i = \{[r_i, v_i]\}$ ,  $i = 1, 2, \dots, K$ ; association cut-off threshold  $e$ 
2  Input:  $prd, e$ 
3  Output:  $prd$ 
4  for  $i = 1 : K - 1$ 
5  for  $j = 1 : K - i - 1$ 
6  if  $abs(prd_i - prd_{i+j+1}) < e$ 
7   $prd = prd_{i+j+1}$ ;
8  end if
9  end for
10 end for

```

---

## 4. Experiments and Results

The detection performance of the proposed algorithm is compared with that of the method outlined in [28]. The quantitative comparison parameters used are as follows.

The average OPSA range measures the accuracy of the number estimation and state estimation of the algorithm for multi-target detection tasks.

The estimation performance is evaluated according to the Optimal Sub-Pattern Assignment (OSPA) range [29]. The true state of the target is represented by  $X = \{x_1, x_2, \dots, x_m\}$ , and the target estimation state is expressed as  $\hat{X} = \{\hat{x}_1, \hat{x}_2, \dots, \hat{x}_n\}$ . Suppose that  $0 < n \leq m$ , then the OSPA is defined as follows:

$$d_{p, c_{cut}}^{OSPA}(X, \hat{X}) = \left( \min_{\pi} \frac{1}{m} \sum_{i=1}^n d_{c_{cut}}(\hat{x}_i, x_i)^p + \frac{c_{cut}^p}{m} (m - n) \right)^{1/p} \quad (16)$$



If  $n > m$ , then  $d_{p,c_{cut}}(X, \hat{X}) = d_{p,c_{cut}}(\hat{X}, X)$ , where  $c_{cut}$  denotes the correlation cut-off radius, the metric norm is defined as  $p \geq 1, \underbrace{\min}_{\pi}$  and denotes all the associations traversed from  $1, \dots, m$  to find the minimum value, and  $d_{c_{cut}}(\hat{x}_i, x_i)$  denotes the cut-off measure, which is defined as  $d_{c_{cut}}(\hat{x}, x) = \min\{c_{cut}, d(\hat{x}, x)\}$ ; here,  $d(\hat{x}, x)$  denotes the benchmark measure of a single objective state  $\hat{x}, x$ .

In simulations, let  $c_{cut} = 1, p = 1$  for the target state analysis containing two-dimensional information of range and Doppler, so the target state error is represented by the following formula:

$$d(\hat{x}, x) = \left[ \frac{1}{2\Delta_r} r, \frac{1}{2\Delta_v} v \right] - \left[ \frac{1}{2\Delta_r} r_{true}, \frac{1}{2\Delta_v} v_{true} \right] \tag{17}$$

The estimation of the target number shows the accuracy of the scenario in which the target number changes. The radar system parameters are provided in Table 1.

**Table 1.** Parameters of the radar system.

Parameter Setting			
	$\Delta_r = 50 \text{ m}$ $\Delta_v = 30 \text{ m/s}$		$R_{max} = 1000 \text{ km}$ $V_{max} = [-300, 300]$
	$f$	$R_{ui}$	$V_{ui}$
$PRF_1$	900 Hz	166.55 km	112.42 m/s
$PRF_2$	1200 Hz	124.91 km	149.89 m/s
$PRF_3$	1500 Hz	99.93 km	187.37 m/s
$PRF_4$	2100 Hz	71.38 km	262.32 m/s

In simulations, the simulation time is set to 100 frames, a maximum of 5 targets is considered at the same time, and the time at which each target appears is  $\{0, 20, 40, 60, 80\}$ . The corresponding initial range and initial velocity of each target are expressed in vector form, as follows:  $\{[600, 200], [600, 125], [700, -500/3], [700, -125], [800, -240]\}$ . According to the standard multi-target observation model, the false alarm setting obeys the Poisson distribution with a parameter of 15. The space obeys the uniform distribution in space. The probability that the target generates a measurement  $P_t$  is 0.85. The Figure 6 shows that the total of 100 frames of measurement sequences according to these parameters.

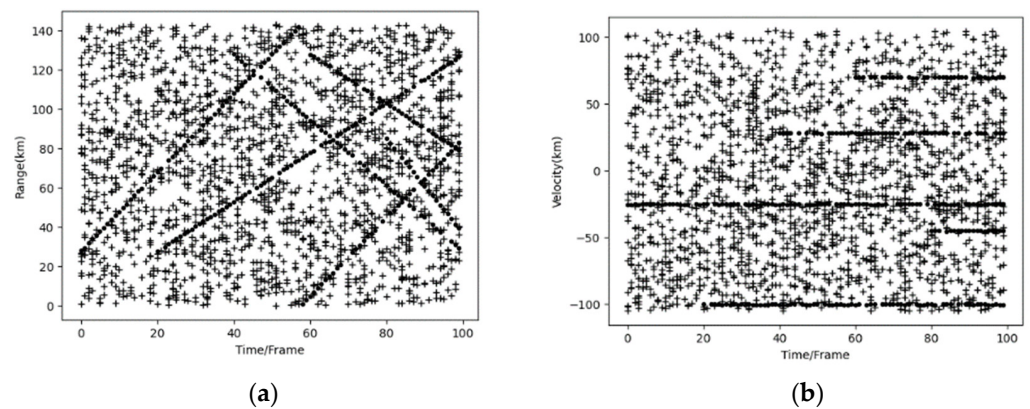


**Figure 6.** The ambiguous measurements under  $PRF = 2100 \text{ Hz}, \lambda = 20$ : (a) range measurements in 100 s; (b) velocity measurements in 100 s.

The horizontal axis represents the number of Monte Carlo trials. '+' represents the false alarms, and '.' represents the measurements from the targets. At each moment, there are a large number of false alarms around the targets. The false alarms and targets are mixed together. The traditional disambiguation algorithm is unable to determine whether the

area component comes from the target or the false alarm; it is also impossible to determine which target the measurement comes from.

Based on the above scenario, in which there is a large detection range, the algorithm is first analyzed under the condition of a fixed clutter rate  $\lambda = 20$ . The different clutter rates are then used to validate the detection and estimation performance of the proposed algorithm.

#### 4.1. Fixed False Alarm Rate

The traditional matrix-based ambiguity resolving method is unable to predict the number of targets; however, in the proposed method, the number of targets is obtained via the detector decision, and the length of the output sequence is set using the known information of the target number. Assuming that there are  $N$  targets, the  $N$  measurement estimation sequences with the smallest error are defined as the prediction states.

The range and Doppler velocity estimation results that were obtained via 100 Monte Carlo experiments are shown in Figure 7.

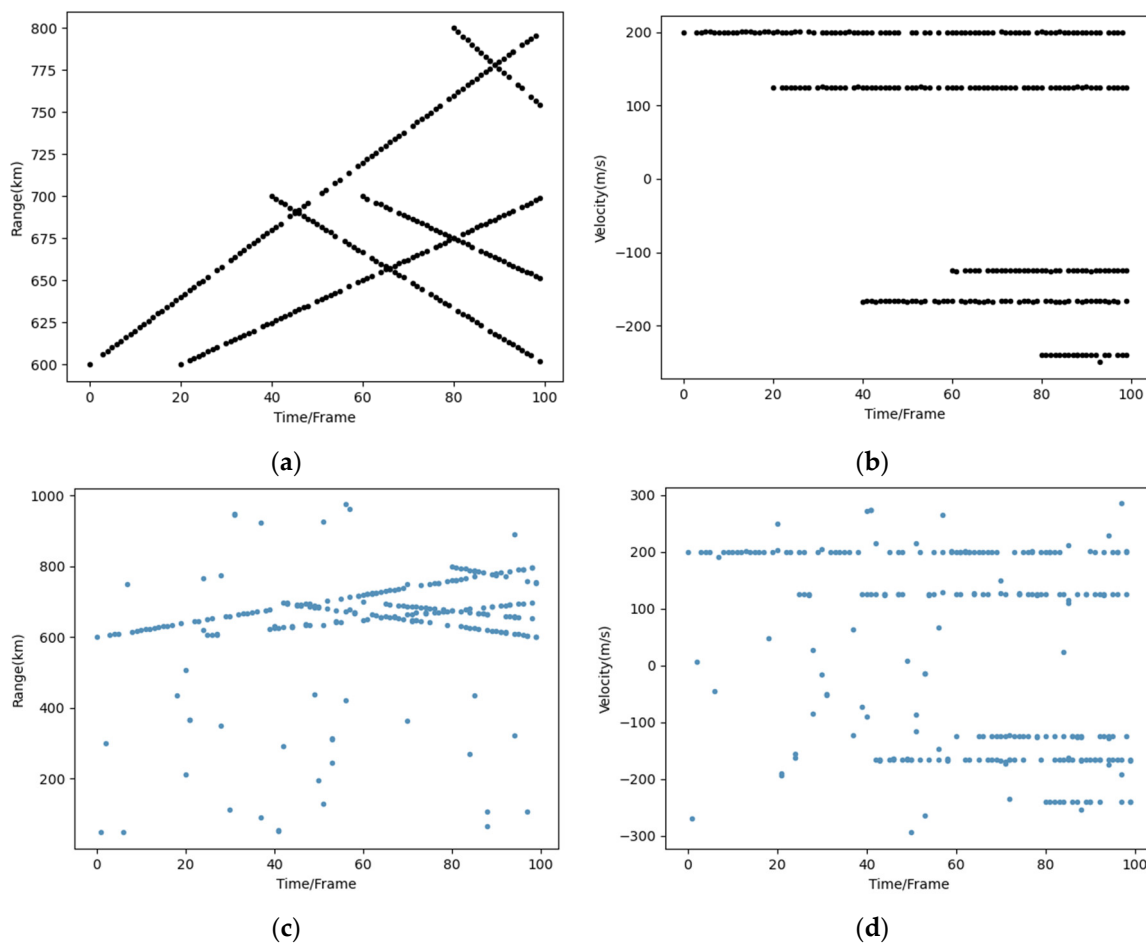


**Figure 7.** The estimation results for the target range dimension and Doppler dimension were obtained using different methods: (a) the range results of the proposed method in 100 s; (b) the velocity results of the proposed method in 100 s; (c) the range results of the traditional method in 100 s; (d) the velocity results of the traditional method in 100 s.

It is evident that the proposed method is superior in its ability to suppress false alarms and is more accurate in its performance of ambiguity resolution. When the number of targets changes, only a few false detections and missed detections occur, especially when the target state is between 80 and 100 frames. Thus, this method has a superior performance. The matrix-based method cannot adapt to the changing target scenario well, resulting in more missed detections.

The average OSPA range is used to further analyze the estimation performance of the algorithm, as shown in Figure 8.

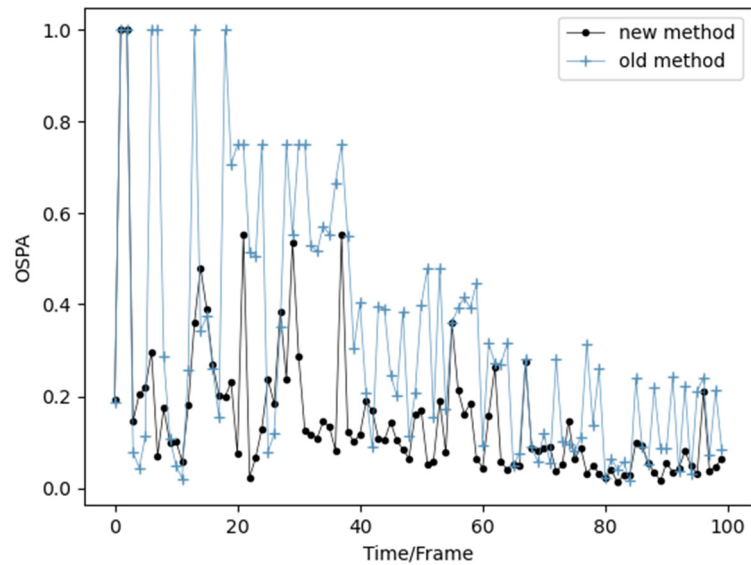


**Figure 8.** The average OSPA distance of the traditional method and the method based on the ambiguity matrix.

Here, the longitudinal axis represents the predicted range and Doppler velocity of the targets, and the transverse axis represents the time/frame.

It can be seen that with the increase in the number of targets, the average OSPA range of the two methods increases, and the method based on the matrix produces more false detections; in turn, this leads to a significantly larger average OSPA distance than the proposed method.

In order to more intuitively explain the detection performance of the algorithm and further analyze the adaptation of the proposed method to the change in the number of targets, Figure 9 shows the estimation of the number of targets by the proposed method.

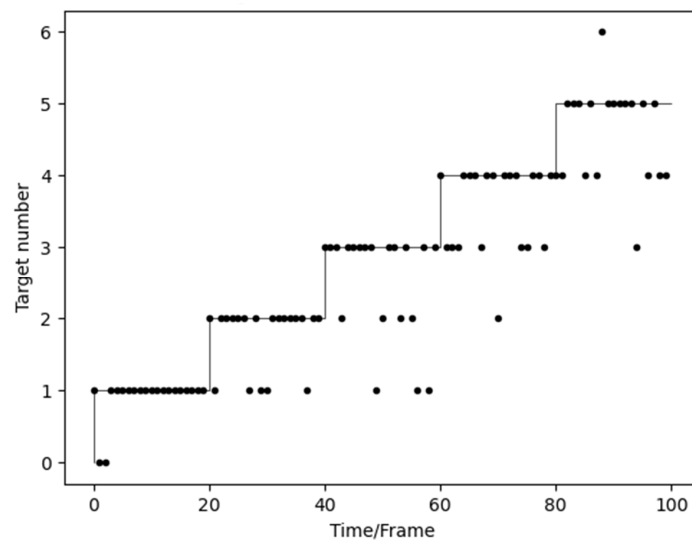


**Figure 9.** The target number estimation of the method based on the ambiguity matrix.

Here, the longitudinal axis represents the target number estimation, and the transverse axis represents the time/frame. The ‘.’ represents the length of target estimation sequences at each frame, and the line represents the actual number of targets at each frame.

#### 4.2. Comparison of Different False Alarm Rate

In order to validate the ability of the proposed algorithm to perform detection and estimation under different clutter rates, the false alarm Poisson distribution parameters of  $\lambda = 20, 40, 60, 80, 100$  are set, and 100 Monte Carlo experiments are carried out. It can be seen from Figure 10 that the proposed algorithm is stronger than the matrix-based method for different clutter rate conditions.

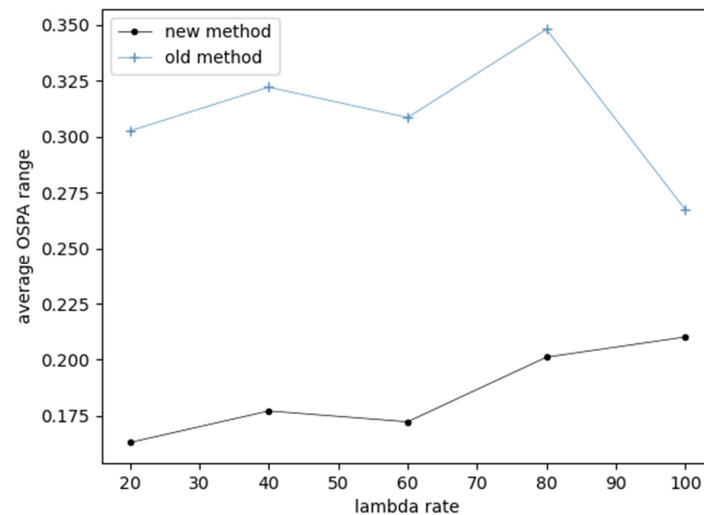


**Figure 10.** The average OSPA range of the proposed algorithm and the method based on the ambiguity matrix.

A comparison of the probability that target detection is achieved by the different methods is shown in Figure 11, in addition to the accuracy of the algorithm in its performance of target detection as the clutter rate increases. In an environment with dense clutter, owing to the strategy of multi-frequency noncoherent accumulation, the algorithm maintains a high probability of achieving target detection; in addition, because the algorithm associates the subsequences, it can effectively deal with the situation in which the target is missing measurements at partial PRFs.

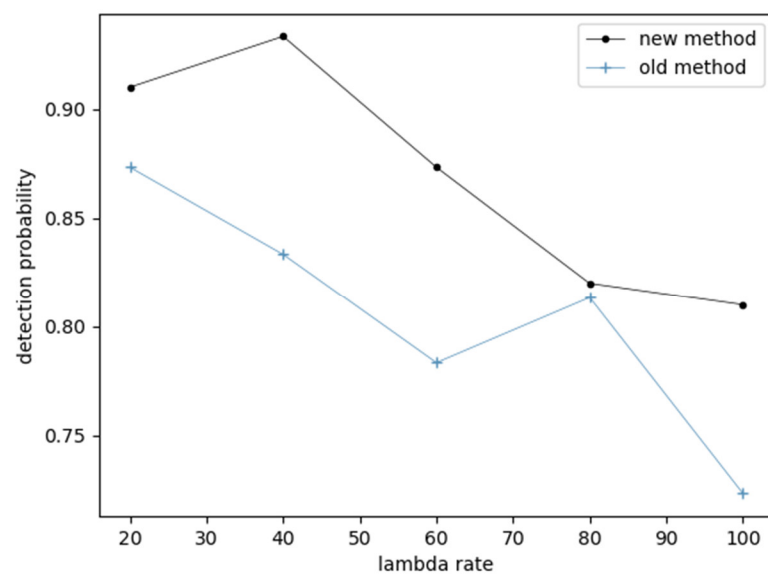


**Figure 11.** The probability that the proposed algorithm and the method based on the ambiguity matrix achieve detection.

## 5. Conclusions

In this paper, an effective method that is able to resolve range–Doppler ambiguity and is based on the ambiguity matrix is proposed; this method then extends the disambiguation to the multi-target task with false alarms. For analysis, we extend the joint detection and ambiguity resolution task to the scenario in which the number of targets changes. The proposed algorithm can adaptively estimate the number of targets and filter out false alarms by using multi-PRF noncoherent accumulation when dealing with a multi-target task in a large detection range.

Numerical simulations have also demonstrated the efficiency of the proposed method. The average OSPA range, estimated target number, detection probability, and other indicators are used to evaluate the number estimation and the measurement error; the proposed algorithm is then compared with the method based on the ambiguity matrix. The qualitative and quantitative experimental results show that the proposed algorithm outperforms other traditional methods in the estimation of multiple targets and the suppression of false alarms. Our future work will focus on multi-target tracking with the problem of ambiguity for the multi-PRF radar system and deal with more challenging tracking scenarios, such as a low SNR.

**Author Contributions:** Conceptualization, Y.M. and C.S.; methodology, Y.M.; software, Y.M.; validation, Y.M. and C.S.; investigation, B.W.; resources, B.W.; writing—original draft preparation, Y.M.; writing—review and editing, C.S.; visualization, C.S.; supervision, B.W.; project administration, B.W.; funding acquisition, B.W. All authors have read and agreed to the published version of the manuscript.

**Funding:** This research received no external funding.

**Data Availability Statement:** No new data were created in this study. Data sharing is not applicable to this article.

**Conflicts of Interest:** The authors declare no conflicts of interest.

## References

1. Li, C.; Ao, L.; Zhou, S.; Feng, H. Overview of payload application of long-endurance stratospheric airship in near space. *Aerosp. Technol.* **2023**, *4*, 80–88. [\[CrossRef\]](#)
2. Silva, B.; Fraidenraich, G. Performance analysis of the classic and robust Chinese remainder theorems in pulsed Doppler radars. *IEEE Trans. Signal Process.* **2018**, *66*, 4898–4903. [\[CrossRef\]](#)
3. Trunk, G.; Brockett, S. Range and velocity ambiguity resolution. In Proceedings of the IEEE Radar Conference, Lynnfield, MA, USA, 20–22 April 1993; pp. 146–149. [\[CrossRef\]](#)
4. Hong, Y. The velocity ambiguity resolution for pulse Doppler radar. *Radar Sci. Technol.* **1995**, *1*, 18–23.
5. Richards, M.A. *Fundamentals of Radar Signal Processing*; McGraw-Hill: New York, NY, USA, 2005; Volume 1.
6. Blackman, S.S. *Multiple-Target Tracking with Radar Applications*; Artech House Publishers: Dedham, MA, USA, 1986.
7. Hovanesian, S.A. Medium PRF performance analysis. *IEEE Trans. Aerosp. Electron. Syst.* **1982**, *3*, 286–296. [\[CrossRef\]](#)
8. Li, X.; Xia, X.; Hong, L. A robust Chinese remainder theorem with its applications in moving target Doppler estimation. In Proceedings of the IEEE Radar Conference, Arlington, VA, USA, 10–14 May 2010. [\[CrossRef\]](#)
9. Zhu, X.; Cui, Z.; Cui, W.; Wu, S. Range and velocity ambiguity resolution based on screening method. In Proceedings of the 2009 IET International Radar Conference, Guilin, China, 20–22 April 2009; pp. 1–3. [\[CrossRef\]](#)
10. Wang, J.; Yang, J.; Wu, S. A New Algorithm of Range Ambiguity Resolution for Pulse Doppler Radar. *Radar Ecm* **2005**, *3*, 38–41.
11. Lin, Z.; Mu, H. MPRF Instrumentation Radar PRF Design. *Syst. Eng. Electron.* **2008**, *30*, 1191–1194.
12. Jiang, K.; Li, M. A Novel Algorithm for PD Radar Range Resolving Ambiguity. *Fire Control Radar Technol.* **2008**, *37*, 25–28.
13. Li, M.; Li, M. A High Efficiency Algorithm of PD Radar for Range Ambiguity Resolution Based on the One-Dimension Method. *Electron. Inf. Warf. Technol.* **2010**, *25*, 22–25. [\[CrossRef\]](#)
14. Hovanesian, S.A. An algorithm for calculation of range in a multiple PRF radar. *IEEE Trans. Aerosp. Electron. Syst.* **1976**, *AES-12*, 287–290. [\[CrossRef\]](#)
15. Qiu, W.; Zhang, D.; Zhao, H. Improvements for Range and Speed Ambiguity Resolving in PD Mode. *Ship Electron. Eng.* **2007**, *27*, 100–102.
16. Wen, L.; Long, T.; Cheng, G.S. The Resolution of Range Ambiguity in a Medium Pulse Doppler Radar. *J. Beijing Inst. Technol.* **1999**, *19*, 357–360.
17. Wen, L.; Long, T.; Han, Y. Resolution of Range and Velocity Ambiguity for a Medium Pulse Doppler Radar. In Proceedings of the Radar Conference, The Record of the IEEE 2000 International, Alexandria, VA, USA, 12 May 2000; pp. 560–564.

18. Zhou, R.; Gao, M.; Dai, Q.; Qingyu, D. Analysis and Simulation for Ambiguity Resolving Using Residues' Difference Look-up Table. *Syst. Eng. Electron.* **2002**, *24*, 30–31.
19. Zhou, R.; Gao, M.; Han, Y. Resolving Ambiguity of Multiple Targets Using Residues' Difference Look-Up Table. *J. Beijing Inst. Technol.* **2002**, *22*, 221–223.
20. Schleher, D.C. *MTI and Pulsed Doppler Radar with MATLAB*; Artech House: Norwood, MA, USA, 2010.
21. Ferrari, A.; Berenguer, C.; Alengrin, G. Doppler ambiguity resolution using multiple PRF. *IEEE Trans. Aerosp. Electron. Syst.* **1997**, *33*, 738–751. [[CrossRef](#)]
22. Liu, Z. Ambiguity resolution for PD radar with remainder theorem and one dimensional set algorithm. *Mod. Electron. Tech.* **2012**, *35*, 28–30. [[CrossRef](#)]
23. Wen, M.; Yi, W.; Wang, Y. Track-Before-Detect Strategies for Multiple-PRF Radar System with Range and Doppler Ambiguities. In Proceedings of the 2018 21st International Conference on Information Fusion (FUSION), Cambridge, UK, 10–13 July 2018; pp. 295–301. [[CrossRef](#)]
24. Vo, B.N.; Mallick, M.; Bar-Shalom, Y.; Coraluppi, S.; Osborne, R.; Mahler, R.; Vo, B.T. Multitarget Tracking. In *Wiley Encyclopedia of Electrical and Electronics Engineering*; Wiley: Hoboken, NJ, USA, 2015.
25. Vo, B.T.; Vo, B.N.; Cantoni, A. The cardinality balanced multi-target multi-Bernoulli filter and its implementations. *IEEE Trans. Signal Process.* **2009**, *57*, 409–423. [[CrossRef](#)]
26. Gao, F.; Zhang, F.; Zhu, H.; Sun, J.; Wang, J. An improved tbd algorithm based on dynamic programming for dim SAR target detection. In Proceedings of the 2014 12th International Conference on Signal Processing (ICSP), Hangzhou, China, 19–23 October 2014; pp. 1880–1884. [[CrossRef](#)]
27. Wang, Z.; Yu, J.; Yang, Y. Resolving Range and Velocity Ambiguity Effectively and Efficiently with GPU. In Proceedings of the 2021 CIE International Conference on Radar (Radar), Haikou, China, 15–19 December 2021; pp. 1122–1126. [[CrossRef](#)]
28. Zhu, J.; Li, Y.; Duan, C.; Wang, W.; Wen, C.; Huang, Y. A Range and Velocity Ambiguity Resolution Method Based on Ambiguity Matrix Completion and Elimination with Low SNR. In Proceedings of the 2019 IEEE International Conference on Signal, Information and Data Processing (ICSIDP), Chongqing, China, 11–13 December 2019; pp. 1–6.
29. Dong, W.; Wu, J.; Song, Z.; Fu, Q. Multi-target joint detection and ambiguity resolving based on adaptive birth density. *J. Signal Process.* **2022**, *38*, 474–482.

**Disclaimer/Publisher's Note:** The statements, opinions and data contained in all publications are solely those of the individual author(s) and contributor(s) and not of MDPI and/or the editor(s). MDPI and/or the editor(s) disclaim responsibility for any injury to people or property resulting from any ideas, methods, instructions or products referred to in the content.